Application of Theoretical Approaches, XRD and XAFS Spectroscopy to Identify Lanthanide Binding Mechanisms in C-S-H Phases

P.Mandaliev[1,2], E. Wieland[1], J. Tits[1], R. Dähn[1], S. Churakov[1]

[1]Paul Scherrer Institut, Villigen PSI, Switzerland; [2]Swiss Federal Institute of Technology (ETH), Zürich, Switzerland

Abstract

Nd(III) binding by xonotlite, a crystalline C-S-H phase, has been investigated using a combination of theoretical approaches, synchrotron-based spectroscopic, and X-ray diffraction techniques. General crystal chemistry arguments and ab initio calculations provided input for the analysis of experimental data obtained from the latter techniques. Synchrotron-based spectroscopic studies were carried out to investigate the local coordination environment of Nd(III) taken up by xonotlite. XRD diffraction studies performed on Nd-doped xonotlite samples allowed changes in the xonotlite structure upon Nd(III) uptake to be determined.

1 Introduction

Cement-based materials play an important role in multi-barrier concepts developed worldwide for the disposal of radioactive wastes [1]. For example, the near field of the planned Swiss repository for long-lived intermediate-level radioactive waste consist to about 90 weight % (wt%) of cement and cementitious backfill materials. Among the different cement phases, calcium silicate hydrates (C-S-H phases) are considered to be the most important with regard to their abundance in cement paste (~50 wt%) and chemically stability in the long term. Thus, C-S-H phases may control the long- term release of radionuclides in repositories for radioactive waste.

The chemical mechanisms governing radionuclide immobilization by amorphous C-S-H phases are poorly known on the molecular level. Development of mechanistic models is difficult due to the lack of long-range order and a high tendency for structural variations of these phases. The interaction of Nd(III) with a crystalline C-S-H-type solid phase, xonotlite ($Ca_6Si_6O_{17}(OH)_2$, molar calcium-to-silicon ratio (C/S) ~1.0) has been investigated with the aim of determining the main structural properties that might control the immobilisation of lanthanides and trivalent actinides by crystalline and amorphous C-S-H phases.

Xonotlite is build up by layers of silica tetrahedra and Ca polyhedra parallel to the b-axis, which represent sheets in the *ab* plane [2]. Ca is sevenfold coordinated in the sheets, or forms distorted octahedra. The silica tetrahedra form a “dreier-doppelkette” structure with 2/m symmetry, which can also be reproduced by two wollastonite-like [Si_3O_9] “dreier-einfachketten” units. Xonotlite has a large number of different polytypes as the silica tetrahedra can be bound to the Ca layer in different, structurally equivalent ways [3].

In this study X-ray absorption fine structure (XAFS) spectroscopy and laboratory-based X-ray diffraction (XRD) techniques were used in combination with atomistic modelling with the aim of investigating the uptake mechanism of Nd(III) by xonotlite. Nd(III) is a non-radioactive redox stable lanthanide. Based on similarities in the complexation behavior of trivalent lanthanides and actinides with comparable ionic radius it is anticipated that Nd(III) is an appropriate chemical analogue for trivalent actinides.

2 Materials and methods

2.1 Synthesis and characterisation of xonotlite

Xonotlite was synthesized by mixing stoichiometric quantities of SiO_2 and CaO powder materials (Ca/Si mol ratio = 1.0) with 220 ml argon-purged Milli-Q water in 250 ml Teflon Parr bombs and heated in a oven at 200°C for 720 hours. The residual paste was dried over saturated $CaCl_2$ solution in a closed container in the glovebox.

The synthesized material was investigated by scanning electron microscopy (SEM), infrared spectroscopy (IR), thermogravimetric analysis (TG/DTA) and X-ray diffraction (XRD) in combination with Rietveld analysis. SEM imaging was carried out using a Zeiss DSM 962 microscope, operated at an accelerating voltage of 20 kV and a beam current of 76 µm. The spot size was ~1x1 μm^2. The microscope is equipped with a Si(Li)-detector for energy dispersive micro-analysis (EDS). IR spectra were recorded in the range 370 cm^{-1} – 5000 cm^{-1} on a Perkin-Elmer 2000 spectrophotometer at room temperature using KBr pellets. TG/DTA was carried out on a Netzsch STA 409 instrument in the range between 30°C and 980°C. The measurements were carried out using about 20 mg of dried xonotlite in an open Al_2O_3 vessel under an argon gasflow (100ml/min) at a heating rate of 20 K/min. The XRD measurements were carried out using a Philips Xpert diffractometer operating in Bragg-Brentano geometry (θ/2θ) and using an XCelerator detector module under normal pressure. The scans were taken between 2θ = 5° and 2θ = 80° at increments of 2θ = 0.017° using Cu $K\alpha_{1,2}$-radiation.

2.2 Sample preparation for XRD and XAFS investigations

XRD was used to investigate Nd-doped xonotlite with high Nd(III) loadings (50000 ppm). Extended X-ray absorption fine structure (EXAFS) measurements were carried out on samples with lower Nd loadings (5000 ppm). Milli-Q water, generated by Millipore water purification system, was used for the preparation of the xonotlite solution with a solid-to-liquid ratio (S/L) of 50 gl^{-1} (pH=10.7). 35 ml aliquots of the vigorously stirred stock suspension were pipetted into 40 ml polyallomere centrifuge tubes (Beckmann Instruments, Inc) and shaken continuously end-over-end. After ageing for one week, appropriate volumes of Nd stock solutions were added to the xonotlite suspensions to achieve the required Nd loadings on the solids. Nd stock solutions were prepared by dissolving Merck “pro analysis” $Nd(NO)_3.6H_2O$ in Milli-Q water (Millipore). Sample preparation was

carried out in a glovebox with controlled N_2 atmosphere (CO_2, O_2 <2ppm, T = 20°C +/- 3°C).

The samples were then shaken continuously end-over-end in the glovebox under controlled N_2 atmosphere. After 1, 14, 30, 60 and 90 days equilibration, phase separation of the solid and liquid phase was carried out by centrifugation (60 min at 95000*g*) using a L7-35 ultracentrifuge (Beckmann Instruments, Inc).

2.3 Quantitative Rietveld analysis

Rietveld analysis allows detailed crystal-structural information from the XRD data to be extracted. In particular, it allows unit cell dimensions (phase chemistry and solid solutions), crystallite size and crystal structure (atomic site occupancy factors) to be determined usually within ±1% uncertainty. Rietveld analysis does require models for the atomic coordinates of all phases present in the sample, which were deduced theoretically using the bond-valence theory or experimentally from X-ray absorption spectroscopy. Details of the method are given elsewhere [4].

Rietveld refinement of synthetic xonotlite was carried out using the GSAS package [5] and the graphical user interface (GUI) editor for GSAS experiment (EXPGUI, [6]). Refinement of synthesized xonotlite was required as up to four polythypes exist simultaneously. As starting model for the Rietveld refinement we used the four known xonotlite polytypes M2a2bc, Ma2bc, M2a2b2c and Ma2b2c (modified Gard notation, respectively space groups P-1, P 2/a, A-1 and A2/a with Ca, Si and O ordered into positions 1h, 1f and 2i (Ca), 1i (Si and O) of P-1, 2i of A-1, 2e of P2/a as well 4c of A 2/a) [3].

2.4 EXAFS spectroscopy

Nd L_{III}-edge (6208 eV) EXAFS spectra were collected at beamline BM26A (DUBBLE, energy range 5 - 30 keV) at the European Synchrotron Radiation Facility (ESRF), Grenoble, France. The beamline is equipped with a Si(111) crystal monochromator. The EXAFS measurements were conducted at room temperature in fluorescence mode using a 9 channel monolithic Ge-solid-state detector. The monochromator angle was calibrated using a Nd foil. Nd-doped xonotlite samples and reference compounds were packed as a wet paste into plexiglas sample holders. The collected data were dead-time corrected. EXAFS data reduction was performed using the WinXAS 3.11 software package following standard procedures [7]. After background subtraction, the energy was converted to photoelectron vector wave units ($Å^{-1}$) by assigning the ionization energy of the Nd L_{III}-edge (6208 eV), E_0, to the first inflection point of the absorption edge. Radial structure functions (RSFs) were obtained by Fourier transforming k^3-weighted χ (k) functions between 2.4-10.3 $Å^{-1}$ with a Bessel window function with a smoothing parameter of 4. Theoretical scattering paths for the fit were calculated using FEFF 8.2 [8] and the structure of the xonotlite polytype M2a2bc as a reference.

3 Theoretical approaches

3.1 Ab initio calculations

The bond-valence treatment of crystal structures requires that the coordinates of all atoms in the system are known. To date, however, the positions of the hydrogen atoms in xonotlite are not known from experimental studies. Therefore, ab initio calculations were carried out to predict the positions of the OH groups in the xonotlite structure. The calculated atomic coordinates have been used as input for the bond valence calculations. The ab initio calculations were performed using density functional plane wave approach implemented in the CPMD package. The exchange and correlation were taken into account by the generalized gradient approximation BLYP [9, 10]. Interaction of the valence electrons with the core states is described by the pseudopotential formalism. We used fully separable norm-conserving pseudopotentials generated using the Troullier-Martin scheme [11]. Because of significant overlap of the valence charge density with the core states of the Ca atoms, the 3s and 3p states were included in the valence. The wavefunctions of valence electrons are expanded into the plane wave basis set up to 70 Ry cut-off energy.

3.2 The bond valence theory

In the bond-valence theory the bond strength (or valence) of an ionic pair is related to their interatomic distance. Atoms are assumed to interact within a first coordination shell only. An inverse power relation between the bond strength and the bond distance holds as the ions approach each other [12. 13].

The bond-valence approach was used to calculate the bond-valence sum that a particular atom would have if it were placed at any arbitrary point in the crystal [12]. Based on this consideration, we were able to identify the places of over-bonded and under-bonded sites in the crystal structure of xonotlite, which form potential sorption sites for Nd(III) (data not shown). With this approach, it was possible to exclude chemically unlike structures and to select the most likely structural configurations as input data in the FEFF8.2 simulations and for structural refinements using Rietveld analysis.

4 Results and discussion

Characterization of the synthesized material (Fig. 1) shows that well crystallized xonotlite formed, further indicating a two-stage process of crystal growth as reported by Shaw and co-workers [14]. First, crystalline phase domains with well ordered periodicity parallel to the *ab* plane and less ordered in the (001) direction form. In this stage of the synthesis the material is very similar to C-S-H gel. In the second stage ordering parallel to c-direction occurs, and the material becomes more ordered. Furthermore, the results of the Rietveld refinement suggest, that all four polytypes are present, but the xonotlite polytype M2a2bc is the dominant phase under the given reaction conditions [15]. This is in good agreement with a recently proposed model for the crystal growth of synthetic crystalline C-S-H phases [14]. Note that the xonotlite polytype M2a2bc (M2a2bc: continuous shift

of monoclinic “unit cells” by +b/4 for stacking in a-direction) is rarely found in natural xonotlite samples, in which the polytype M2a2b2c (M2a2b2c: continuous shift of monoclinic “unit cells” by +b/4 for stacking in a-direction and shift of +b/2 for stacking in c-direction) is dominant.

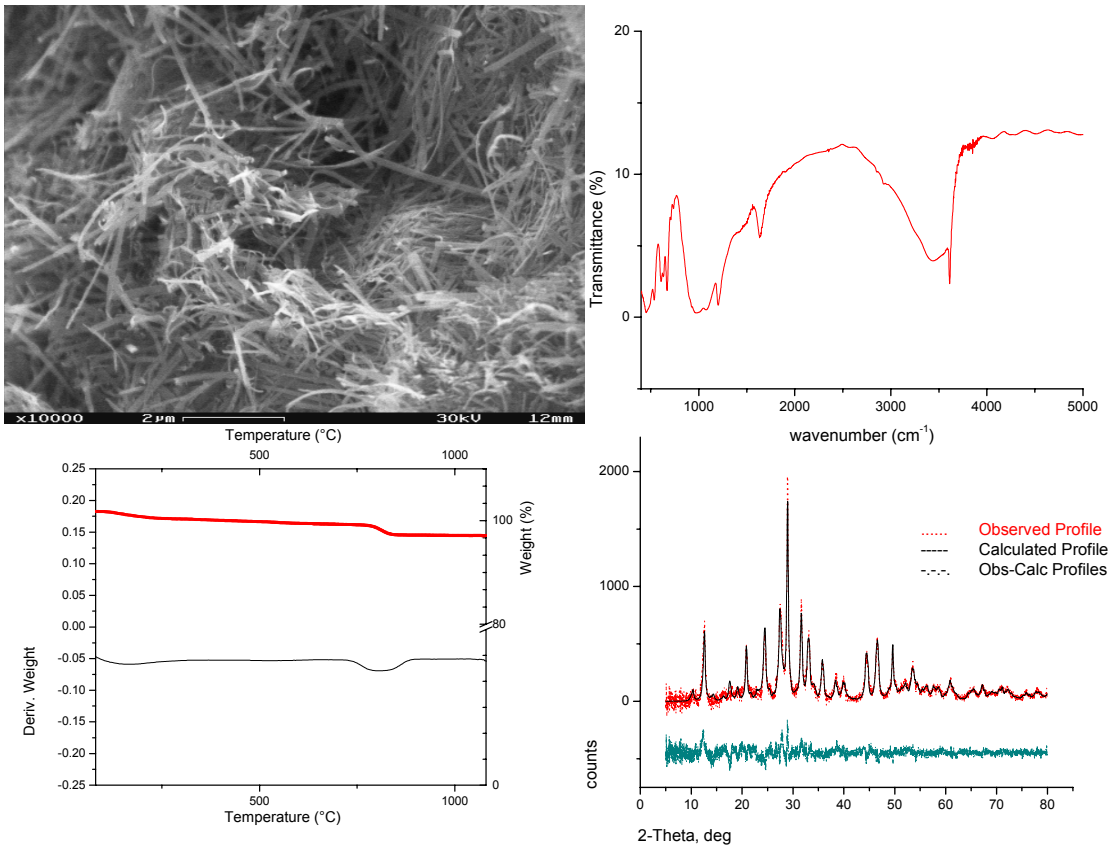

Figure 1 Synthetic xonotlite: a) SEM image; b) Infrared spectrum (370 - 5000 cm^{-1}); c) TG/DTA scan (30°C and 980°C; d) XRD pattern and Rietveld analysis (obs-calc profile corresponds to the residual of the Rietveld refinement).

Fig. 2a shows the normalized, background subtracted, and k^3-weighted EXAFS spectra of Nd-doped xonotlite samples equilibrated for different time periods. Fig. 2b shows that the RSFs of all samples display a major peak at about R+ΔR ~2.0 Å, which corresponds to the contribution of the nearest O shells. Furthermore, the broad peaks at R+ΔR ~3.0 Å indicate backscattering contributions from further shells. The FT peak at about 2.0 Å was fitted by assuming the presence of a single oxygen shell. The coordination number was determined to be about 8, and R_{Nd-O}=2.44 Å, which is shorter than R_{Nd-O}=2.51Å in $Nd(OH)_3$ (Fig 2c and 2d). This finding suggests that the formation of $Nd(OH)_3$ in these systems can be excluded. This conclusion was further supported based on the comparison of the

spectra, showing that the spectra of the xonotlite samples differ from those of $Nd(OH)_3$ (data not shown).

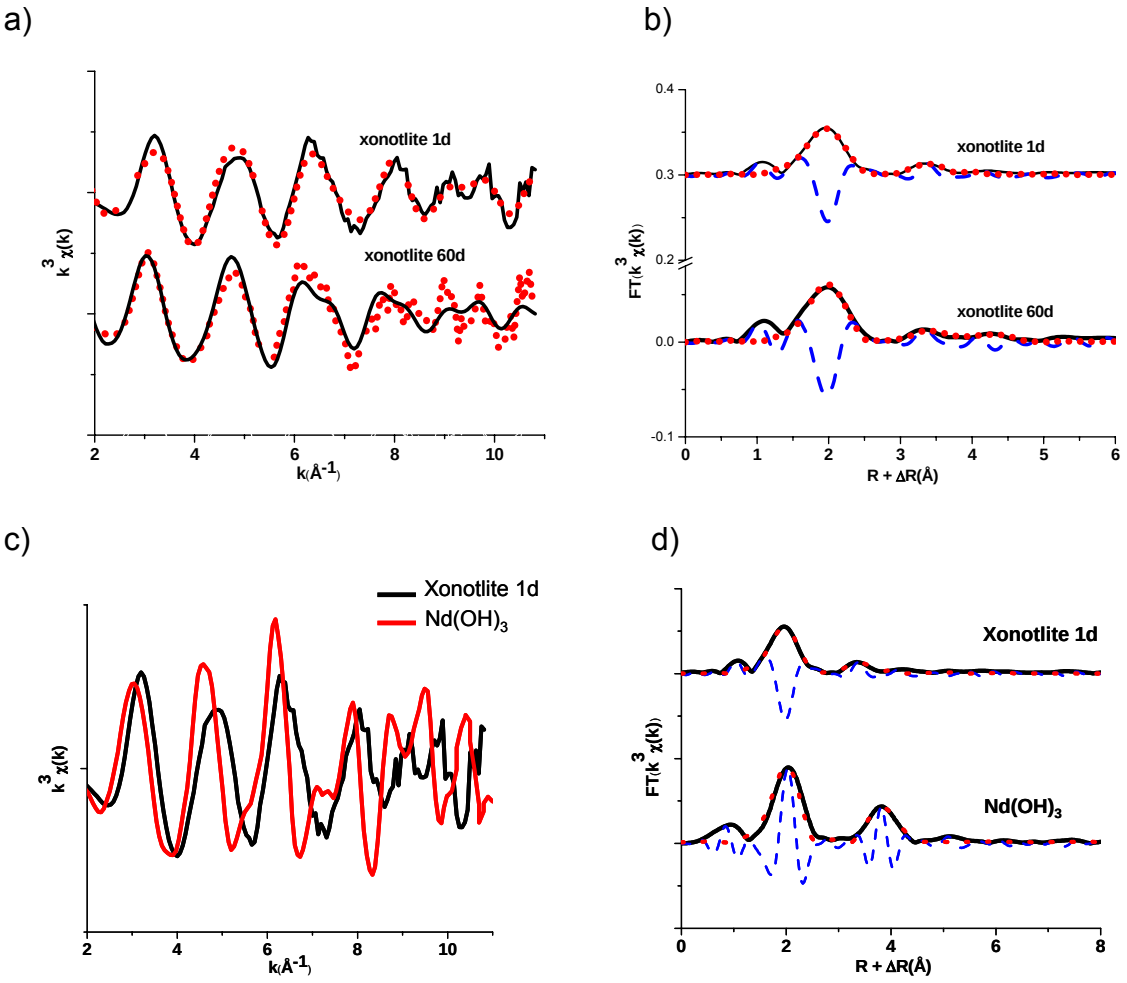

Figure 2 a) k^3-weighted, normalized, background subtracted EXAFS spectra for Nd-doped xonotlite samples equilibrated for 1 and 60 days. Solid line: experimental data; dotted line: modeled data, b) Experimental (solid line) and theoretical Fourier transforms (dotted line: modulus; broken line: imaginary part) obtained from EXAFS spectra, c) k^3-weighted, normalized, background subtracted EXAFS spectra for Nd-doped xonotlite samples equilibrated for 1 and $Nd(OH)_3$, d) Experimental (solid line) and theoretical Fourier transforms (dotted line: modulus; broken line: imaginary part) obtained from EXAFS spectra of xonotlite samples equilibrated for 1 and $Nd(OH)_3$

Table 1 Structural information[a] obtained from Nd K-edge data analysis.

	Nd-O			Nd-Si			Nd-Ca			Nd-Ca			
Eq. (d)	N	R (Å)	σ^2 ($Å^2$)	N	R (Å)	σ^2 ($Å^2$)	N	R (Å)	σ^2 ($Å^2$)	N	R (Å)	σ^2 ($Å^2$)	ΔE_0 (eV)
1	8.1	2.45	0.01	6.0	3.66	0.005	6.5	3.74	0.005	2.12	4.0	0.005	6.5
60	6.4	2.42	0.009	4.5	3.66	0.005	5.1	3.73	0.005	1.36	3.9	0.005	5.0

[a] N, R, σ^2 and ΔE_0 stand for the coordination number, inter-atomic distance, Debye-Waller factor, and inner potential correction. Note that the Debye-Waller factors of the second and higher shells were linked to each other. The residuals (%) indicating the deviation between experimental data and fit given by the relative residual in percent were determined to be 10.8 and 10.2, respectively. (%res = $((\sum_{i=1}^{N} \left| y_{exp}(i)-y_{theo}(i) \right|)/(\sum_{i=1}^{N} y_{exp}(i)))\cdot 100$, with N = number of data points, y_{exp} and y_{theo} = experimental and theoretical data points, respectively).

It should be noted that a distance of R_{Nd-O}=2.44 Å for the Nd-doped xonotlite samples compares well with average Nd-O distances of known neodymium-silicate compounds [R_{Nd-O}=2.42-2.48 Å] [16, 17].

Fitting of further neighboring shells showed, after one day equilibration, Si and two Ca backscattering contributions (Nd-Si: R = 3.66 Å, N = 6.0; Nd-Ca: R = 3.74 Å, N = 6; Nd-Ca: R = 3.93 Å, N = 2). Table 1 indicates that the coordination number of Nd(III) in the Nd-doped samples determined after 60 days of equilibration are lower than those after one day contact time, i.e., the initial coordination numbers N_{Si} ~6 and N_{Ca} ~6.5 and 2, respectively, change to N_{Si} ~4.5 and N_{Ca} ~5 and 1.4, respectively. However, the same bond distances resulted within the uncertainty range, i.e., the initial distance R_{Nd-Si} = 3.66 Å remains unchanged, and the Nd-Ca distances slightly changed: R_{Nd-Ca} = 3.73 Å and 3.93 Å instead of R_{Nd-Ca} = 3.74 Å and 3.95 Å. This indicates that the coordination environment of Nd did not significantly change with time.

The structural parameters listed in Table 1 suggest that Nd(III) is bound in structure of a solid phase. This idea was further substantiated by XRD measurements on Nd-doped xonotlite (see below) The solid phase could be a mixed surface precipitate or solid solution with xonotlite, respectively. However, it should be noted that EXAFS spectra represent an averaged signal from all individual Nd species bound to xonotlite. Therefore, at the present time, we can not rule out that two or more species with different coordination environment could account for the observed spectra. Further investigations are needed to determine the number of surface species formed in this system.

The XRD patterns of Nd-doped xonotlite are shown in Fig.3. Bragg peaks, which are unique to xonotlite and correspond to the (001) and (200) planes, have been observed. The intensities and the half-widths of these peaks are listed in Table 2. The first reflection (001), which is characteristic for xonotlite, represents the space between the Ca layers. This range further includes the position of the silanol groups (Si-OH) as calculated from the molecular dynamics simulations. The second reflection (200) indicates the plane parallel to the c-direction, according to the stacking sequence of the monoclinic unit cells. As shown in Fig. 3 the intensity of the (200) peak and the half-width of this peak did not change with time, indicating stability of the xonotlite structure in c-direction (Table 2). In contrast, the intensity of the (001) peak decreases and the relative half-width of the peak increases with increasing equilibration time, indicating increasing disordering in the space between the Ca layers. Additional changes in the XRD pattern were observed: The intensities of the peaks at $2\theta=27.5°$ and $2\theta=33.2°$, corresponding to the crystallographic planes (102) and (202), decrease and the relative half-widths of the peaks increase with time. By contrast, the Bragg peaks that are typical for poorly crystalline C-S-H phases at $2\theta=28.9°$ and $2\theta=31.7°$ remain with regard to intensity and relative half-width. The results from XRD measurements suggest that, with time, the structural order of xonotlite is reduced and Nd-doped xonotlite becomes more amorphous. This finding can be rationalized in terms of the sequential phase transition between C-S-H → xonotlite proposed by Shaw and co-workers [14]: C-S-H → C-S-H-Gel → 11Å tobermorite → xonotlite. This process is reverse in the case of the Nd-doped xonotlite, giving rise to decreasing intensities of those reflections that are characteristic for xonotlite. Further, this interpretation agrees with the finding that reflections characteristic for poorly crystalline C-S-H remain unchanged.

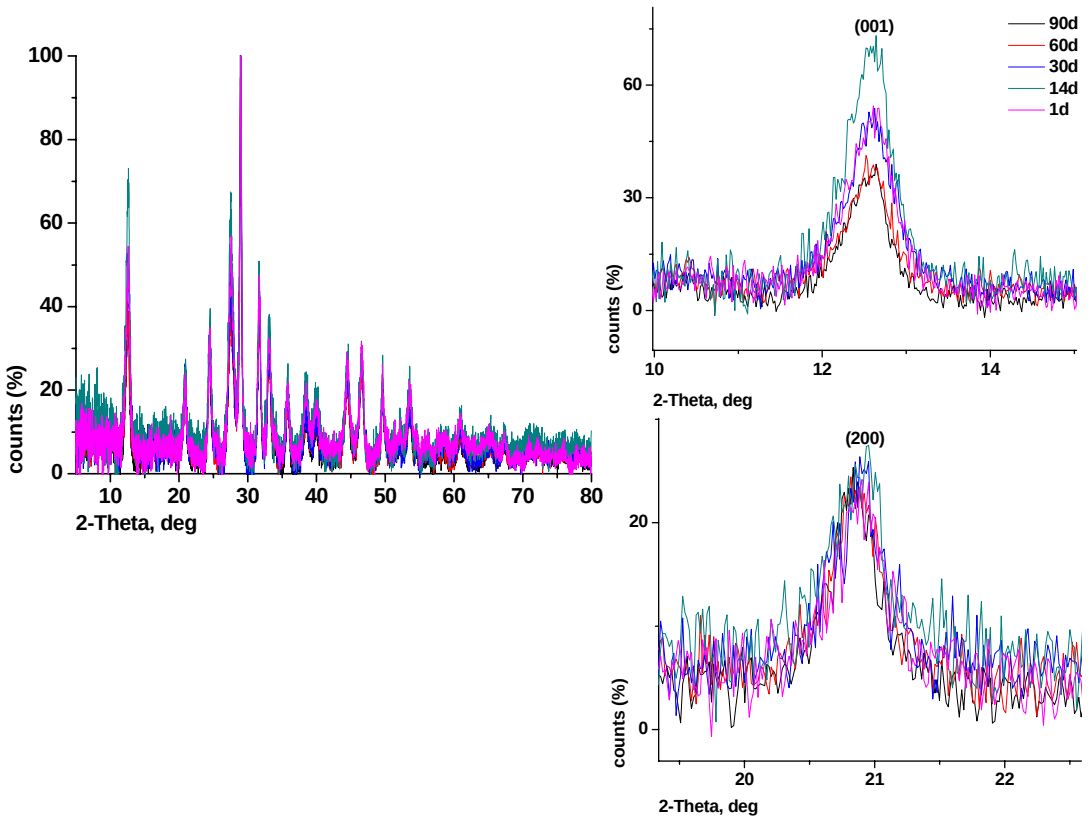

Figure 3 XRD of Nd-doped xonotlite sample equilibrated between 1 and 90 days (see Table 2). The peak intensities corresponding to the (200) and (001) crystallographic planes are listed in Table 2.

Table 2 Peak intensities and half-widths of XRD reflections (001) and (200).

Equilibration (days)	(001) Intensity (%)	(001) Half-Width (deg)	(200) Intensity (%)	(200) Half-Width (deg)
1	73	1.7	21	1.6
14	54	1.7	21	1.6
30	50	1.8	21	1.6
60	40	1.8	21	1.6
90	35	1.9	21	1.6

The results from the XRD measurements further revealed that the observed XRD pattern is different from those of $Nd(OH)_3$ (data not shown). This finding agrees with the earlier conclusions drawn based on the EXAFS results. Therefore, both methods show that the formation of $Nd(OH)_3$ can be excluded in these systems in contrast to predictions made from solubility calculations. This finding indicates that Nd(III) is rapidly taken up by xonotlite. The significant changes observed in

the XRD pattern further show that Nd(III) is bound in the structure of xonotlite. This finding suggests that, in agreement with our interpretation of the EXAFS data, Nd(III) may interact with xonotlite to form a solid solution or mixed surface precipitation.

5 Conclusion

Nd(III) uptake by xonotlite has been investigated using a combination of theoretical approaches (ab initio molecular dynamics simulations and bond-valence calculation), synchrotron-based spectroscopic and laboratory-based X-ray diffraction techniques. Theoretical calculations allowed the exact positions of the OH groups in xonotlite to be determined, which are thought to balance the bond valance of Nd(III) bound in the xonotlite structure. The data from EXAFS measurements can be interpreted in terms of the formation of a solid solution. At the present time, however, we can not rule out that different Nd(III) surfaces species exist in these systems. XRD investigations on Nd-doped xonotlite with high Nd loadings show significant changes in the xonotlite structure with time. Structural ordering of xonotlite decreases, indicating the formation of a less crystalline solid phase. This finding, together with the EXAFS results, suggests that, in fact, Nd(III) is bound in the structure of xonotlite.

The present study shows that the uptake of Nd(III) by crystalline C-S-H phases can be successfully studied using the proposed combination of different techniques. Analysis of (EXAFS) spectroscopy data yields molecular crystal-chemical information and is applicable at low metal loadings (e.g. 5000ppm and below). Unlike, XRD in combination with Rietveld analysis requires sufficiently high Nd(III) loadings on the solid phases (>50 000ppm metal loadings). This combined approach is currently applied to investigate Nd(III) uptake by tobermorite. In contrast to xonotlite the latter phase has a Ca interlayer, and therefore, the solid is considered to be an appropriate structural model for aged C-S-H phases with low Ca/Si ratios.

6 Acknowledgements

The staff of the beamlines BM26 (DUBBLE) at ESRF, Grenoble, France, and microXAS at SLS, Villigen PSI, Switzerland, is thanked for the experimental assistance during the synchrotron-based investigations. Thanks are extended to Dr. E. Curti, D. Kunz and Dr. M. Vespa (PSI) for assistance during the measuring campaigns. Dr. F. Winnefeld (EMPA, Switzerland) provided measuring time and experimental assistance with the XRD measurements and his contribution to this project is gratefully acknowledged. Thanks are extended to R. Brütsch, A. Frei and Dr. R. Koetz (PSI) for assistance during the SEM, TG/DTA and IR investigations. Partial financial support was provided by the National Cooperative for the Disposal of Radioactive Waste (Nagra), Switzerland.

7 References

[1] N. Chapman, C. McCombie, Principles and standards for the disposal of long lived radioactive waste, Pergamon, Amsterdam, 2003.

[2] Garbev, K. (2004). Structure properties and quantitative Rietveld analysis of calcium silicate hydrates crystalyzed under hydrothermal conditions., Forschung Zentrum Karlsruhe**:** 271.

[3] C. Hejny, T. Armbruster, Polytypism in xonotlite $Ca_6Si_6O_{17}(OH)_2$. Z. Kristallogr. 216 (2001) 396-408.

[4] R.A. Young, The Rietveld method, IUCr Monographs on Crystallography 5, Oxford University Press, Oxford, UK, 1993.

[5] Larson, A.C. and Von Dreele, R.B. (1994) General structure analysis system (GSAS). Los Alamos National Laboratory Report LAUR B6-748, Los Alamos, New Mexico.

[6] Toby, B. H. (2001):EXPGUI, a graphical user interface for GSAS, J. Appl. Cryst.. 34, 210-213

[7] T. Ressler, WinXAS: A programme for X-ray absorption spectroscopy data analysis under MS-Windows, J. Synchrotron Rad., 5, 118-122.

[8] J.J. Rehr, J. Mustre de Leon, S.L. Zabinsky, R., C., Albers, Theoretical X-ray absorption fine structure standards, J. Am. Chem. Soc. 113 (1991) 5135-5140.

[9] Becke, A. D. (1988). "Density-functional exchange-energy approximation with correct asymptotic behavior." Physical Review A 38(6): 3098-3100.

[10] Lee, C., W. Yang, et al. (1988). "Development of the Colle-Salvetti correlation-energy formula into a functional of the electron density." Physical Review B 37(2): 785-789.

[11] Troullier, N. and J. L. Martin (1991). "Efficient pseudopotentials for plane-wave calculations." Physical Review B 43: 1993-2006.

[12] Brown, I.D. Altermatt, D. (1985): Bond-Valence parameter obtained from a systematic analysis of the inorganic crystal structure database. Acta Cryst. B41, 244-247

[13] Brese, N.E., O'Keefe, M. (1991): Bond valence parameters for solids. Acta Cryst.. B 47, 192-197

[14] S. Shaw, S.M. Clark, C.M.B. Henderson, Hydrothermal formation of the calcium silicate hydrates, tobermorite ($Ca_5Si_6O_{16}(OH)_2{\cdot}4H_2O$) and xonotlite ($Ca_6Si_6O_{17}(OH)_2$): an in situ synchrotron study, Chem. Geol. 167 (2000) 129-140.

[15] Churakov and Mandaliev, 2006 (in preparation)

[16] A.V. Chichagov, N.V. Belov, The crystal structure of $NaNdSiO_4$. Geokhimiya. (1968) 1456-1461.

[17] Smolin, Yu.I., Shepelev, Yu. I. (1970) The crystal structure of the rare earths pyrosilicates. Acta. Cryst., B, 26, 484-492.